1 Science Justification

1.1 Cluster Mass Mapping

The mass distribution in galaxy clusters is a crucial test of our cosmological paradigm. Total halo masses probe the amplitude of matter fluctuations and growth of structure in the Universe, and the abundance of substructure within halos is sensitive to the history of hierarchical assembly and potentially the interaction cross section of dark matter (e.g., Natarajan et al., 2002a,b; Voit, 2005; Clowe et al., 2006). Gravitational lensing has played an important role in mapping dark matter within halos, primarily by exploiting the distortion of images of background galaxies. On small scales inside lensing clusters, strong distortions produce extended arcs and multiple images enabling the production of detailed mass maps, while on larger scales the distortions are weaker and require averaging the shapes of many background galaxies over a broad area to extract a shear signal.

We propose to map the projected mass distribution in the massive cluster Abell 2261 with a new lensing techinque that uses kinematic measurements of background sources to drastically improve the signal-to-noise (S/N). The typical weak lensing shear signal averaged within the virial radius of a massive cluster ($\gamma_t \sim 0.05$) is small compared to the distribution of intrinsic shapes in imaging (which has scatter $\sigma_\gamma \sim 0.25$). Kinematic information can be used to infer the intrinsic shape and orientation of the background galaxies, potentially reducing the shape noise per galaxy by a factor of ten. This enables S/N $\gtrsim 1$ measurements of shear with individual galaxies. With such precision we will improve the spatial resolution of mass maps and extend the precision of strong lensing out to the weak regime near the virial radius of the cluster. We discuss this technique and its potential for improving both the precision and accuracy of future large-scale lensing experiments in the next section. Additionally, the repeat slit spectra taken for hundreds of sources behind A2261 will provide two-dimensional kinematics of emission line disk galaxies, greatly enhancing the sample size at that redshift for studying evolution of galaxy kinematics and the Tully-Fisher relation (TFR).

1.2 Kinematic Weak Lensing

The utility of kinematic maps for weak lensing was originally described by Blain (2002) and Morales (2006), who forecasted constraints from high S/N, high spatial resolution observations with future radio arrays. The basic idea for the kinematic shear observables is described in Figure 2. In an image, an inclined rotating circular disk has elliptical isophotes. When the image of this galaxy is sheared, the isophotes remain elliptical (in the weak shear limit, $|\gamma_t| \ll 1$) with a new axis ratio and position angle. New photometric axes are inferred from this ellipse in the sheared image, and information about the original axes is lost. The case is different however, with kinematic measurements. The unsheared circular disk has kinematic axes that are perpendicular to one another and are aligned with the unsheared photometric axes. This cross shape becomes skewed when the velocity map is sheared; the kinematic axes are no longer perpendicular and they are misaligned with the photometric axes inferred from the sheared isophotal ellipse in the imaging data.

Full two-dimensional kinematic maps are not required for this measurement, and our approach adds to the previous discussion by incorporating information from the TFR, an empirical scaling relation for disk galaxies between their luminosity and circular velocity $v_{\rm circ}$. With slit spectroscopy, the measured amplitude of a rotation curve is related to the true circular velocity by $v_{\rm obs} = v_{\rm circ} \sin i$, where i is the inclination of the disk toward the observer. Thus the offset between $v_{\rm obs}$ and $v_{\rm circ}$ predicted from the TFR gives a kinematic estimate of $\sin i$. Typically observers estimate $\sin i$ from the ellipticity of the image. The difference between the photometric and kinematic estimates of $\sin i$ gives an estimate of the shear.

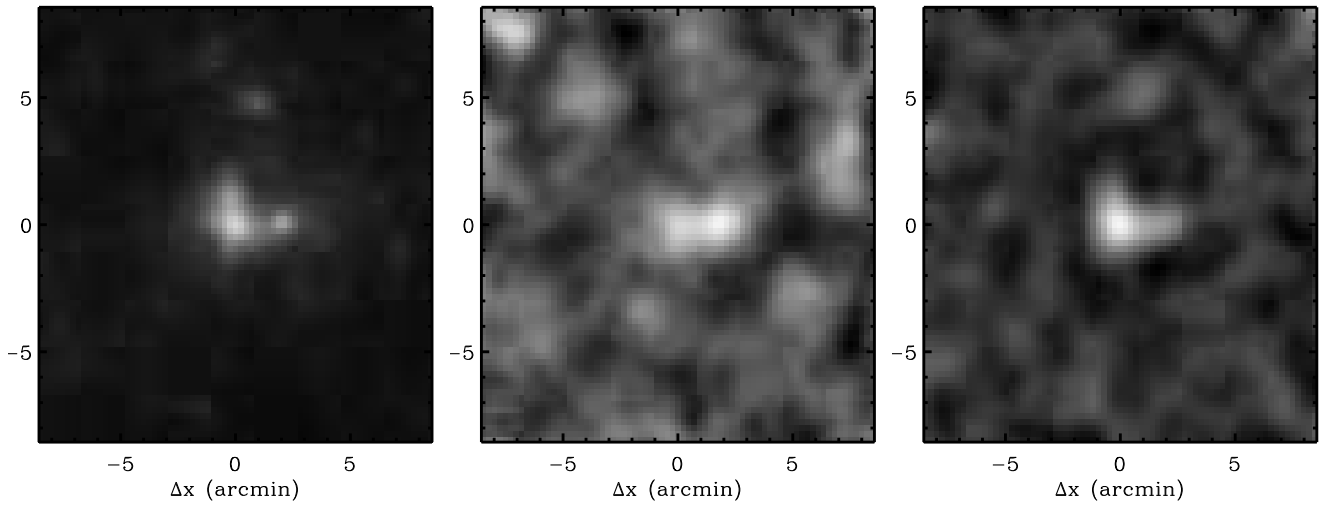

Figure 1: **Left:** mass map, from Vale & White (2003) simulations, zoomed in on a distended $10^{15} M_{\odot}$ cluster. **Center:** Aperture mass map with shape noise properties equivalent to existing Subaru observations of A2261. **Right:** Aperture mass map with shape noise properties equivalent to proposed TFR lensing survey. Aperture scale is tuned for each map to optimize signal-to-noise and resolution. Peak κ values are approximately .07 for both maps.

For ideal circular disks, the shear can be measured to arbitrary precision, limited only by the spatial and spectral resolution of the data. In practice, the intrinsic scatter of the TFR limits the precision of the shear measurement. After inclination correction, estimates for the intrinsic fractional scatter in $v_{\rm circ}$ at fixed luminosity or stellar mass are typically $0.05 - 0.06$ dex both locally and to $z \sim 1.3$ (Reyes et al., 2011; Miller et al., 2011). For a properly weighted estimator of the galaxy shape based on the TFR offset, this scatter maps to an uncertainty in the intrinsic galaxy ellipticity of only $\sigma_{\epsilon,\rm TFR} = 0.015$. This should be compared to the intrinsic shape noise for pure disks $\sigma_{\epsilon,\rm disks} = 0.59$ and for real imaging surveys $\sigma_{\epsilon,\rm im} \approx 0.4$, and is related to the shear noise through $\sigma_\epsilon / \sigma_\gamma \approx 2(1 - \sigma_\epsilon^2)$(Bernstein & Jarvis, 2002; Hirata et al., 2004). This quantity is sensitive to measurement errors in $v_{\rm circ}$, as shown in Figure 3; in general, rotation curve errors of < 10 km/s reduce the disk galaxy shape noise by an order of magnitude.

1.3 A Pilot Study for Future Dark Energy Experiments

In addition to its uses in mapping individual structures, statistical weak lensing over wide fields is also a major science driver for several ongoing and future cosmology experiments, ranging from the ongoing Dark Energy Survey and Kilo-Degree Survey projects to space missions like Euclid and the Wide-Field Infrared Survey Telescope. The errors in these surveys are likely to be dominated by systematic errors arising from the necessity of using photometric redshifts for the sources and the difficulties in obtaining unbiased shape measurements for galaxies near the detection limit. In addition to its primary science goals described above, this proposal is also a pilot study, informing our understanding of the viability of kinematic weak lensing over wide fields with the next generation of fiber-fed massively multi-object spectrographs. Instruments such as the planned MS-DESI or Subaru Prime Focus spectrographs are expected to achieve target densities similar to those we propose to obtain here, but over thousands of square degrees. If even crudely resolved kinematics can be obtained by these instruments, it may be possible perform wide-field kinematic weak lensing measurements that significantly exceed even future space missions in their weak lensing signal-to-noise, while avoiding the aforementioned sources of systematic bias that remain highly problematic for existing lensing studies. In addition to its primary cluster science goals, this proposal serves an useful role as a pilot study for a hypothetical wide-field spectroscopic lensing experiment.

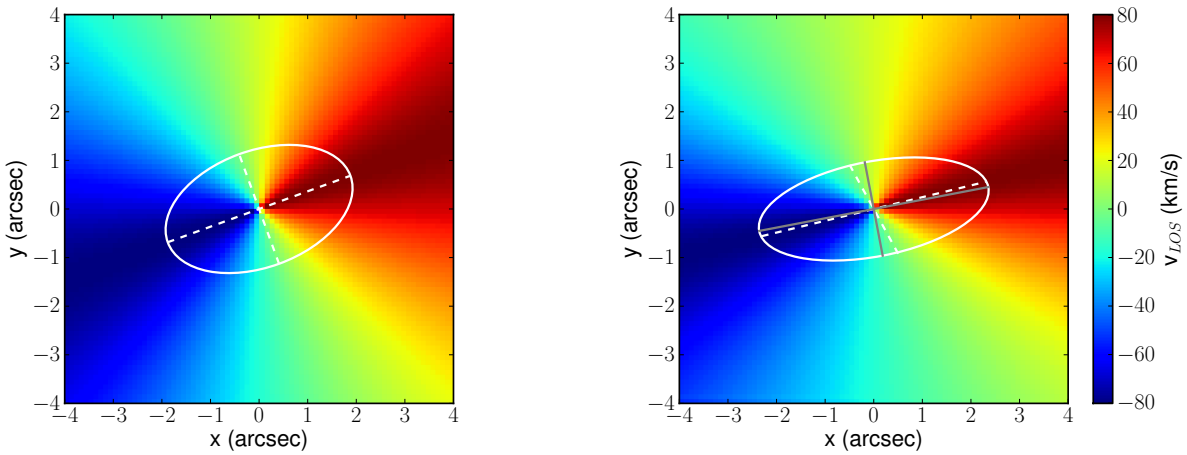

Figure 2: Effects of shear on kinematic maps of an inclined disk galaxy. Color maps show velocity map, and white contours show a single image isophote. A shear applied at 45° to the disk major axis misaligns the kinematic and image axes. Effect is shown for an exaggerated shear with amplitude $|\gamma|$=0.1

1.4 2-d Disk Kinematics at $z \sim 0.5$

2 Technical Remarks

2.1 Targets and Exposures

Abell 2261 ($z = 0.225$, Coe et al. 2012) is an ideal target for testing this novel mass mapping technique since its high mass ($M_{\rm vir} \approx 2.2 \times 10^{15}\,M_\odot$) and moderate redshift produces a large lensing signal for background galaxies at $z \sim 0.6 - 1.2$, and its angular size $R_{\rm vir} \approx 3\,{\rm Mpc} = 13.4'$ is well-matched to the DEIMOS field of view. We propose to cover this cluster with 4 slit masks, with most of the area covered twice by perpendicular masks to allow repeat observations of targets with $\Delta P.A. = 90°$ (Figure 4). This will enable us to measure velocities along both photometric axes to better constrain the shear.

Abell 2261 is part of the CLASH sample (Postman et al., 2012) which obtained multi-wavelength HST data for the inner $\sim 3'$ and has existing Subaru data in B, V, and R bands. We will target galaxies behind the cluster using a BVR color selection modeled on the DEEP2 BRI selection (Newman et al., 2013) which successfully identified a large sample of high redshift galaxies and measured rotation curves using the [OII] emission line. To resolve the [OII] doublet, we will use the 1200 line/mm grating. The line flux needed for measuring kinematics with the DEIMOS configuration used by DEEP2 is $\gtrsim 10^{-17}\,{\rm erg/s/cm^2}$ (Kassin et al., 2012). Using COSMOS data (Jouvel et al., 2009), we find that a BVR color selection from Subaru photometry with a target density of $1.5 - 2\,{\rm arcmin^{-2}}$ can efficiently select resolved ($r_{1/2} > 0.5$") galaxies at $z \sim 0.6 - 1.2$ with [OII] fluxes above this threshold. This strategy should produce a sample of > 100 galaxies with two-dimensional kinematics measured at $z \sim 0.9$. To ensure sufficient S/N in velocity measurements along both axes, we request **2 hour exposures × 4 masks = 8 hours shutter time**. [Morphology cuts?]

2.2 Backup Program

2.3 Supplementary Observations

2.4 Status of Previously Approved Keck Programs

The following sections are optional but highly recommended

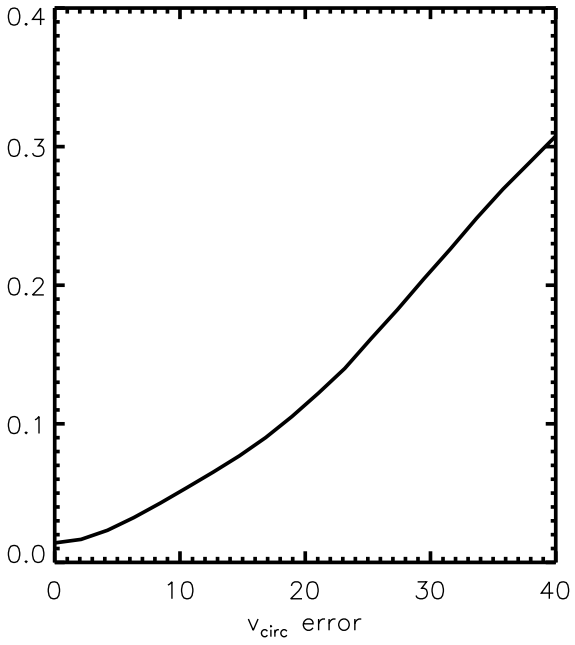

Figure 3: Effective shape noise σ_{TF} as a function of the measurement error on the disk circular velocity.

2.5 Path to Science from Observations

2.6 Technical Concerns

2.7 Experience and Publications

2.8 Resources and Publication Timescale

References

Bernstein, G. M., & Jarvis, M. 2002, AJ, 123, 583

Blain, A. W. 2002, ApJL, 570, L51

Clowe, D., Bradač, M., Gonzalez, A. H., Markevitch, M., Randall, S. W., Jones, C., & Zaritsky, D. 2006, ApJL, 648, L109

Coe, D., et al. 2012, ApJ, 757, 22

Hirata, C. M., et al. 2004, MNRAS, 353, 529

Jouvel, S., et al. 2009, A&A, 504, 359

Kassin, S. A., et al. 2012, ApJ, 758, 106

Miller, S. H., Bundy, K., Sullivan, M., Ellis, R. S., & Treu, T. 2011, ApJ, 741, 115

Morales, M. F. 2006, ApJL, 650, L21

Natarajan, P., Kneib, J.-P., & Smail, I. 2002a, ApJL, 580, L11

Natarajan, P., Loeb, A., Kneib, J.-P., & Smail, I. 2002b, ApJL, 580, L17

Newman, J. A., et al. 2013, ApJS, 208, 5

Postman, M., et al. 2012, ApJS, 199, 25

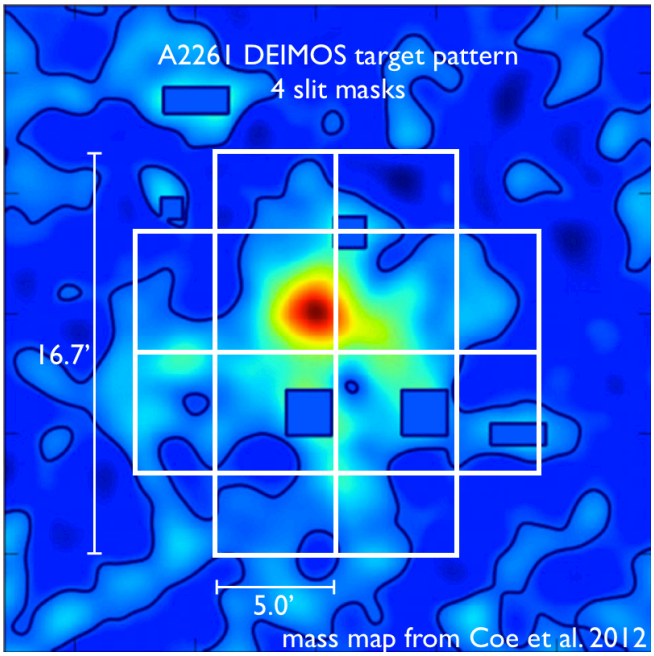

Figure 4: Mass map of A2261 , with proposed DEIMOS slitmask geometry superposed.

Reyes, R., Mandelbaum, R., Gunn, J. E., Pizagno, J., & Lackner, C. N. 2011, MNRAS, 417, 2347

Vale, C., & White, M. 2003, ApJ, 592, 699

Voit, G. M. 2005, Reviews of Modern Physics, 77, 207